Broad-Area High-Power Top Surface Emitting Laser Diodes

Martin Grabherr

Top surface emitting vertical-cavity lasers with active diameters from 4 to 150 μm have been investigated to estimate the limits of maximum cw output powers for single devices.

1. Introduction

In the past few years, performance of vertical-cavity surface-emitting laser diodes (VCSELs) has been improved dramatically. Threshold current densities and threshold voltages are as low as 200 A/cm^2 [1] and 50 mV [2] above corresponding bandgap voltages, respectively. Wallplug efficiencies exhibit 50 % [3, P-54] for small device diameters of around 6 μm. With maximum output powers of a few mW these devices are well suited for optical data transmission. Maximum output power is limited by thermal roll over and thus by dissipated power, which can be minimized by low series resistances of the Bragg reflectors and current apertures formed by selective oxidation of AlAs layers reducing nonradiative recombinations. High optical output powers should now be attainable with broad-area devices.

2. Device Structure

A schematic of the investigated devices is depicted in Fig. 1. P- and n-type Bragg reflectors surround the active region consisting of 3 InGaAs quantum wells, GaAs barriers, and AlGaAs cladding layers. On top of the mesa a TiPtAu ring forms the p-type contact, whereas GeNiAu is evaporated on the substrate as n-type contact. The devices are attached junction up to a copper block using silver paste. Substrate thickness is around 400 μm. The copper block can be heated or cooled in order to control heat sink temperature.

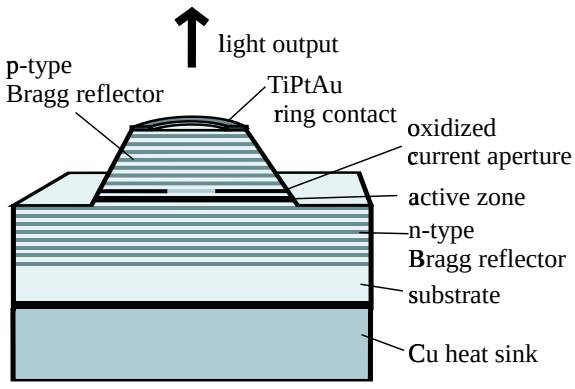

Fig. 1. Cross section of a top emitting VCSEL mounted junction up on copper heat sink.

3. Fundamental Characteristics and Modeling of Output Powers

To estimate attainable output powers for top surface emitting VCSELs, simple modeling of output power as a function of laser current i has been chosen according to

$$P = \hbar\omega/q \cdot \eta_d \cdot (i - i_{th}) \cdot f(\Delta T) \quad , \tag{1}$$

where $\hbar\omega$ denotes the photon energy, q is the electron charge, η_d the differential quantum efficiency, and i_{th} the threshold current. Laser heating is taken into account by the function $f(\Delta T)$ and the intrinsic temperature rise ΔT can be determined from the thermal resistance and the dissipated power as

$$\Delta T = R_{th} \cdot P_{diss} \quad . \tag{2}$$

Assuming a linearized current-voltage characteristics with a constant differential resistance R_d and a kink voltage V_k, the dissipated power is written as

$$P_{diss} = (V_k + R_d \cdot i) \cdot i - P \quad . \tag{3}$$

From the experiments, the parameters i_{th}, R_{th}, and R_d can all be expressed as functions of the device diameter D_{act} and therefore output power is now only a function of driving current and laser size. The intrinsic temperature rise ΔT cannot be directly measured, therefore the thermal resistance in (2) has to be calculated from the quotients of wavelength shifts $\Delta\lambda$ with both dissipated power ΔP_{diss} and heat sink temperature T_{hs} as

$$R_{th} = \frac{\Delta\lambda}{\Delta P} \left(\frac{\Delta\lambda}{\Delta T_{hs}} \right)^{-1} \quad . \tag{4}$$

Fig. 2 depicts the wavelength shift with dissipated power for a 150 μm active diameter device, showing a high degree of linearity. The device emits in multiple transverse modes among which a single mode has to be recorded with an optical spectrum analyzer to obtain the wavelength shift. This procedure is also applied for observing the red shift with increasing heat sink temperature for constant dissipated power in Fig. 3, which directly gives the slope of wavelength deviation with intrinsic temperature. Due to the dependence of refractive indices on temperature, this

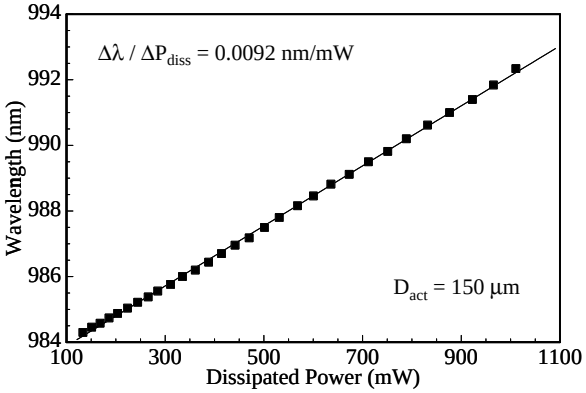

Fig. 2. Wavelength shift with dissipated power for a 150 μm diameter device.

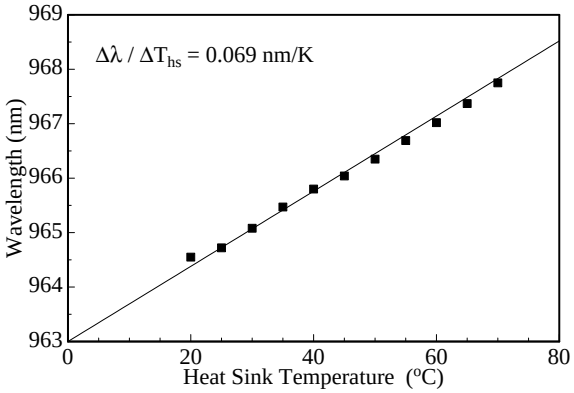

Fig. 3. Tuning of the emission wavelength with varying heat sink temperature.

slope is constant for all devices with identical layer structure independent of the active diameter. For the given example a thermal resistance of 133 K/W is calculated. Measurements for device diameters from 4 to 150 μm result in an inversely proportional behavior of thermal resistance with device diameter in accordance with a simple theoretical model [4] in which the thermal resistance is related to the thermal conductivity λ_c by

$$R_{th} = \frac{1}{2\lambda_c D_{act}} \quad . \tag{5}$$

A fit to the experimental data, shown in Fig. 4, determines λ_c to 40.4 W/(m·K) which is close to the value 44 W/(m·K) usually taken for the GaAs substrate material. Using a resistance network

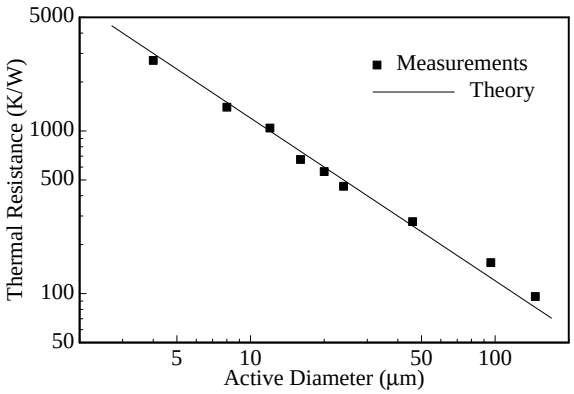

Fig. 4. Thermal resistance of top surface emitting VCSELs versus device diameter.

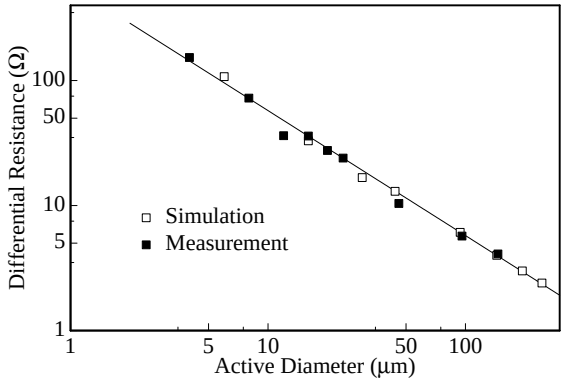

Fig. 5. Differential resistance of the investigated devices as a function of avtive diameters.

model [5], series resistances for investigated device structures, contact geometries, and doping concentrations have been simulated. The results for a broad range of device diameters are in good agreement with the measurements as seen in Fig. 5. Again we see an inversely proportional dependence with active diameter, which is not directly expected because of the increase of the active area with D_{act}^2. This effect can be explained by current crowding at the oxide aperture with a circumference being proportional to D_{act}. The dependence in Fig. 5 ca be fitted with a single parameter as

$$R_d = \frac{575\ \Omega\mu\mathrm{m}}{D_{act}} \quad . \tag{6}$$

Another input parameter for the simulation is the threshold current versus active diameter, depicted in Fig. 6. Again it is expected that the threshold current increases with the squared diameter, but this is only confirmed for device sizes below 40 μm. For larger diameters an almost linear increase is seen from the measurements, again being due to the inhomogeneous current density distribution in the active area. To describe the thermal behavior of the output characteristics, the temperature T_{off} at the thermal turn off point is calculated from the light-current curves presented in Fig. 7. We obtain an almost constant value $T_{off} = 200\,^{\circ}\mathrm{C}$ for all device sizes and for different heat sink temperatures T_{hs}. The function describing thermal behavior in the simulation is simply assumed to be

$$f(\Delta T) = 1 - \frac{\Delta T + T_{hs}}{T_{off}} \quad , \tag{7}$$

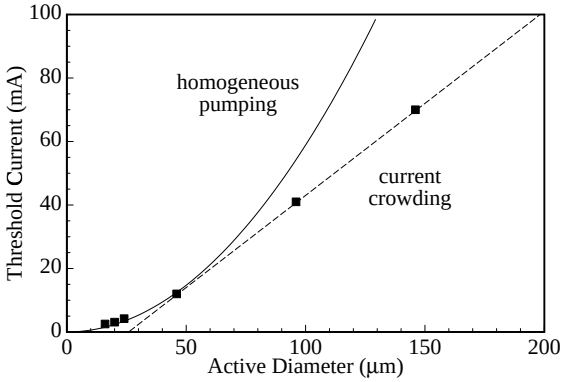

Fig. 6. Threshold current versus device diameters.

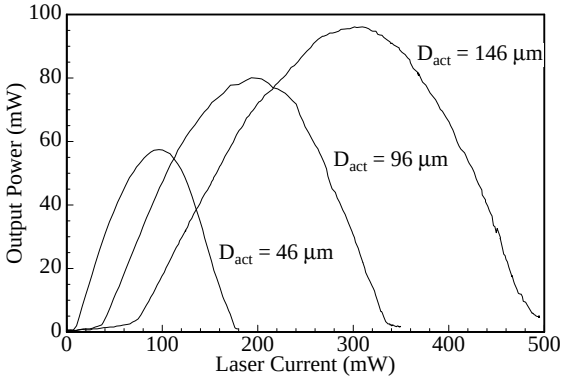

Fig. 7. Output characteristics and thermal turn off for different device diameters.

taking a constant heat sink temperature into account and enforcing $P = 0$ at $T = T_{off}$ while neglecting temperature dependencies of all other parameters.

4. Comparison of Modeling and Measurements

Taking the emission wavelength of 990 nm and a differential efficiency of 90 % into account, the output characteristics can be simulated using equations (1)–(3) and the experimental data according to (5)–(7) and Fig. 6. The good agreement between measurement and simulation in Fig. 8 for a 50 μm device confirms the assumptions used in the model. For this device maximum wallplug efficiency is 40 % at 40 mW output power. Maximum output power at thermal roll over is 78 mW. Performing these simulations for various device diameters, a linear increase of maximum output power with device diameter is expected, as plotted in Fig. 9. The experimental data only show a sublinear increase due to the injection of carriers near the center of the active region where mo stimulated emission occurs. Maximum wallplug efficiencies are as high as 40 % for device sizes up to 50 μm and decrease down to 20 % for devices with 150 μm active diameter.

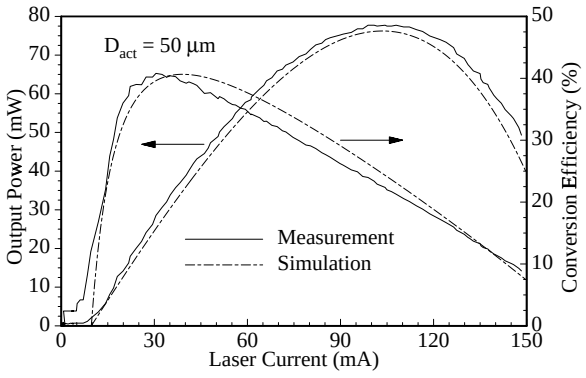

Fig. 8. Comparison of measured and simulated output characteristics of a 50 μm active diameter device.

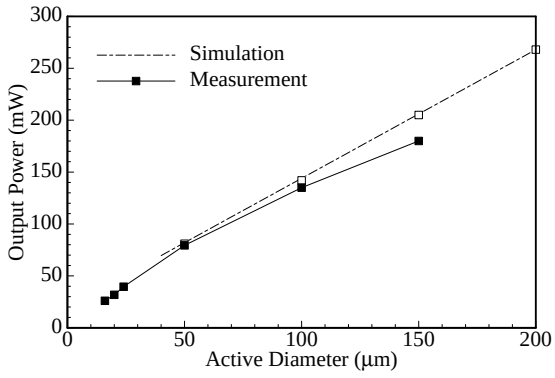

Fig. 9. Maximum output power for different device sizes.

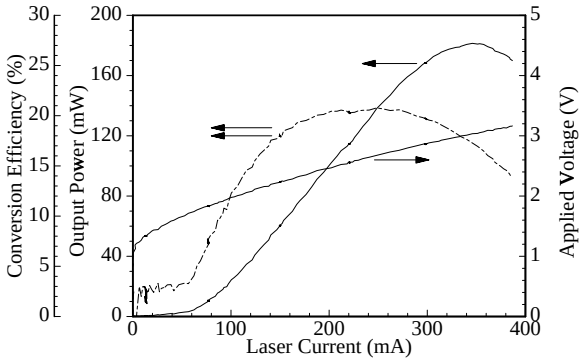

Fig. 10. CW output characteristics of a device with 150 μm active diameter.

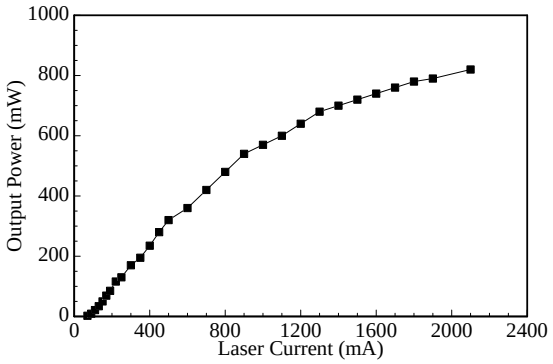

Fig. 11. Pulsed operation with maximum pulse power of 820 mW of the device from Fig. 10.

5. Maximum Output Powers for CW and Pulsed Operation

The characteristics of the devices with the highest cw output power experimentally observed are presented in Fig. 10. At a laser current of 350 mA, 180 mW output power is reached at room temperature with a wallplug efficiency of 15 %. The broad current range where high conversion efficiency is obtained is due to the low series resistance of 3.8 Ω and an optimized tuning of resonance wavelength and gain peak. Therefore 160 mW output power is achieved at maximum wallplug efficiency of 20 %. Fig. 11 shows the importance of further improvements of mounting technologies and thus reductions of thermal resistance. Pulsed operation results in 820 mW output power at 2.1 A current for a pulse width of 1 μs and a duty cycle of 1:100. The relatively large pulse width and accompanied heating still gives rise to the power saturation seen in Fig. 11.

6. Outlook

Further reductions of dissipated power by decreasing the differential resistance and more homogeneous current density distributions are expected for bottom emitting devices. Together with junction down soldering of those devices and thus lower thermal resistances, higher output powers for VCSELs are foreseeable.

References

[1] P. D. Dapkus, M. H. MacDougal, G. M. Yang, A. E. Bond, C. Lin, D. Tishinin, V. Pudikov, Y. Cheng, and K. Uppal, "Ultralow threshold current lasers", in Proc*Conf. on Lasers and Electro-Optics CLEO'96*, Anaheim, CA, USA, pp. 357–358, 1996.

[2] K. D. Choquette, R. P. Schneider, Jr., K. L. Lear, and K. M. Geib, "Low threshold voltage vertical-cavity lasers fabricated by selective oxidation", *Electron. Lett.*, vol. 30, pp. 2043–2044, 1994.

[3] K. L. Lear, K. D. Choquette, R. P. Schneider, Jr., S. P. Kilcoyne, and K. M. Geib, "Selectively oxidised vertical-cavity surface-emitting lasers with 50 % power conversion efficiency", *Electron. Lett.*, vol. 31, pp. 208–209, 1995.

[4] W. Nakwaski and M. Osinski, "Thermal resistance of top-surface emitting vertical-cavity semiconductor lasers and monolithic two-dimensional arrays", *Electron. Lett.*, vol. 28, pp. 572–574, 1992.

[5] R. Michalzik and K. J. Ebeling, "Modeling and design of proton-implanted ultralow-threshold vertical-cavity laser diodes", *IEEE J. Quantum Electron.*, vol. 29, pp. 1963–1974, 1993.